Ceramics International xxx (xxxx) xxx

Contents lists available at ScienceDirect

Ceramics International

journal homepage: www.elsevier.com/locate/ceramint

Investigation of magnetic and non-magnetic mechanisms for the attenuation of superconductivity in manganite/cuprate multilayers

Chao C. Zhang [a], Min Gu Kang [b], Riccardo Comin [b], John Y.T. Wei [a,*]

[a] Department of Physics, University of Toronto, 60 St. George St., Toronto, M5S 1A7, Canada
[b] Department of Physics, Massachusetts Institute of Technology, 77 Massachusetts Avenue, Cambridge, MA, 02139, USA

ARTICLE INFO

Handling Editor: P. Vincenzini

Keywords:
Oxide superconductors
Interfaces
Superconductivity
Films

ABSTRACT

We investigate the role strain-induced deoxygenation plays on the observed T_c attenuation in multilayers of $La_{1/3}Ca_{1/3}MnO_3$ (LCMO) and $YBa_2Cu_3O_{7-\delta}$ (YBCO), where a long-range ferromagnetic/superconductor proximity effect is proposed to exist. We compare changes to the superconducting T_c in several sets of oxygen-underdoped perovskite/YBCO/perovskite trilayers, where the perovskite layers consist of LCMO; $LaNiO_3$ (LNO), which is structurally similar to LCMO but non-magnetic; and $PrBa_2Cu_3O_{7-\delta}$ (PBCO), which is both non-magnetic and better lattice-matched with YBCO. We find that LCMO and LNO trilayers show similar T_c attenuation in response to decreasing annealing pressure. We also use x-ray absorption spectroscopy to directly gauge the hole concentration (p) in LCMO trilayers, where we find both thinner YBCO layers and greater oxygen underdoping decreases p. Our results indicate that strain-induced deoxygenation of the YBCO layer by itself can account for the observed T_c attenuation in LCMO/YBCO multilayers.

1. Introduction

Epitaxial multilayers of the cuprate superconductor $YBa_2Cu_3O_{7-\delta}$ (YBCO) and the half-metallic manganite $La_{1/3}Ca_{1/3}MnO_3$ (LCMO) exhibit many phenomena not present in their constituent layers [1–5]. One such phenomenon is a dependence of its superconducting transition temperature (T_c) with changing YBCO and LCMO layer thicknesses at unexpectedly long (up to 40 nm) length scales [2]. This length scale is several orders of magnitude longer than the length scale predicted by a "conventional" ferromagnetic/superconductor (F/S) proximity effect (~0.7 nm) [2]. A proposed explanation for this anomalous length scale is the existence of a long-range F/S proximity effect in the system [2], which likely necessitates the proximitized Cooper pairs to have spin-triplet and odd-frequency components in their wave function [6–9]. However, no spectroscopic evidence of any F/S proximity effect has been observed in *c*-axis LCMO/YBCO bilayers at the theoretically proposed length scales [10].

Another proposed explanation for this long-range T_c attenuation involves the heteroepitaxial strain between the YBCO and LCMO layers. In *c*-axis LCMO/YBCO multilayers, heteroepitaxial strain induces double-chain intergrowths within YBCO [11,12]. The lattice-symmetry mismatch between the two materials (pseudo-cubic LCMO and orthorhombic YBCO) favours the formation of these intergrowths [11]. The compressive strain on the *b*-axis of the YBCO layer also deoxygenates it to match the tetragonal LCMO better [13]. Since the epitaxial strain is still present at up to 200 nm from the epitaxial interface [14–17], its effects can also explain the length scale of the observed T_c attenuation. Previous studies [11,12] explicitly show similar T_c attenuation as the YBCO thickness is decreased in both LCMO/YBCO/LCMO trilayers and trilayers of $LaNiO_3$ (LNO) and YBCO. Since LNO is a paramagnetic cubic perovskite with comparable lattice parameters as LCMO [18,19], these prior studies indicate that heteroepitaxial strain, rather than any magnetic effects unique to LCMO, is primarily responsible for the observed T_c suppression in LCMO/YBCO multilayers [12].

This study aims to explore the extent strain-induced deoxygenation of YBCO is responsible for the observed T_c attenuation in LCMO/YBCO/LCMO trilayers and to probe the relative magnitudes of any magnetic mechanisms on T_c compared to strain-induced changes to the doping level (p) [13,20,21]. To isolate the effects of deoxygenation from that of magnetism, we compare the T_c attenuation in deliberately oxygen-underdoped LCMO/YBCO/LCMO and LNO/YBCO/LNO trilayers (LCMO and LNO trilayers respectively). Since $PrBa_2Cu_3O_{7-\delta}$ (PBCO) has a comparable orthorhombic lattice as YBCO, we also

* Corresponding author.
E-mail address: wei@physics.utoronto.ca (J.Y.T. Wei).

https://doi.org/10.1016/j.ceramint.2023.01.234
Received 31 August 2022; Received in revised form 30 January 2023; Accepted 30 January 2023
Available online 1 February 2023

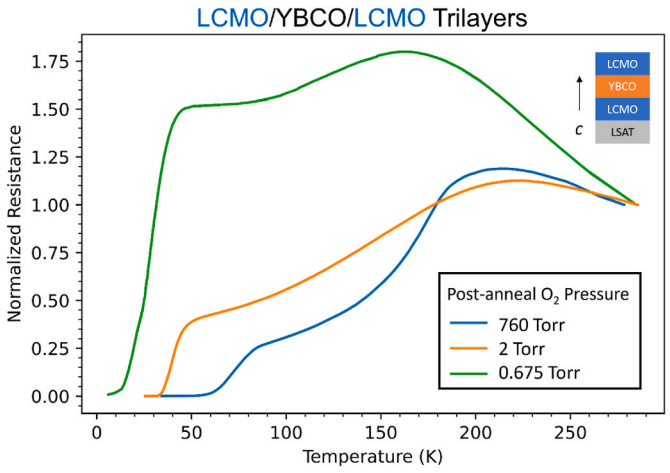

Fig. 1. Normalized R vs. T plots of LCMO trilayers with 10 nm LCMO and YBCO layers. The exact trilayer layout is shown in the inset. The R curves are normalized through division by the room temperature R value of the corresponding trilayer. Peak structures associated with the Curie temperature of the LCMO layers are present for all three curves. A superconducting transition is also visible in all three curves, with the superconducting transition occurring at progressively lower temperatures as the annealing pressure is lowered. Similarly, the transition becomes progressively broader with lower annealing pressures.

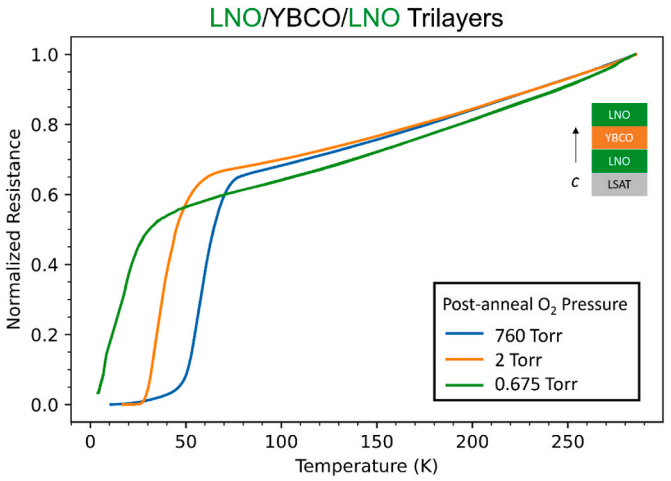

Fig. 2. Normalized R vs. T plots of LNO trilayers with 10 nm thick LNO and YBCO layers. The exact trilayer layout is shown in the inset. The R curves are normalized through division by the room temperature R value of the corresponding trilayer. Superconducting transitions are visible in all three samples, where the T_cs of the LNO trilayers are similar to those seen in similarly-annealed LCMO trilayers.

measure and compare the T_c attenuation of similarly treated PBCO/YBCO/PBCO trilayers (PBCO trilayers) for a non-magnetic and lattice-matched control. A trilayer geometry is chosen for the samples to emulate the unit cell of the LCMO/YBCO superlattice and to symmetrize the epitaxial strain on the YBCO layer. In this series of comparisons, we find that similarly-underdoped LCMO and LNO trilayers exhibit similar T_c s. In contrast, the PBCO trilayers show significantly milder T_c attenuation as a function of oxygen underdoping. The p values of several LCMO trilayers are also measured using x-ray absorption spectroscopy (XAS) to measure their hole concentration (p) directly. We find p decreases with decreasing YBCO layer thickness as well as increasing YBCO layer oxygen underdoping. These results indicate that the observed T_c attenuation in LCMO trilayers can solely be accounted for by strain-induced deoxygenation of the YBCO layer.

2. Material and methods

Trilayers were grown on $(LaAlO_3)_{0.3}(Sr_2TaAlO_6)_{0.7}$ (LSAT) and $SrTiO_3$ (STO) substrates using pulsed laser-ablated deposition (PLD). LSAT was used as the substrate for the LCMO and LNO trilayers, while STO was used as the substrate for the PBCO trilayers. LCMO and LNO trilayers were grown on LSAT because its in-plane lattice constant (3.868 Å) is well matched with that of LCMO (3.86 Å) and LNO (3.82 Å). Similarly, PBCO trilayers were grown on STO because the in-place lattice constant of STO (3.905 Å) is well matched with both in-plane axes of PBCO (3.86 and 3.91 Å respectively). PLD growth was done using a 248 nm KrF excimer laser with a fluence of 2J/cm^2. LCMO and LNO trilayers were grown using a substrate temperature of 800 °C and a 0.2 Torr O_2 chamber pressure, while PBCO trilayers were grown using a substrate temperature of 750 °C and the same 0.2 Torr O_2 chamber pressure. The LCMO, LNO, and PBCO layers were set at thicknesses of 10 nm, while the thickness of the YBCO layer was varied. Layer thicknesses were set using material-specific growth rates. These growth rates were determined using atomic force microscopy (AFM) on chemically etched single-layer films and corroborated using x-ray reflectometry (XRR) measurements. After growth, all trilayer films were annealed in situ by cooling at 10 °C/min from the growth temperature to 450 °C. The samples are then held at 450 °C for 2 h before the sample heater is shut off. Oxygen underdoping of the YBCO layer is achieved by reducing the O_2 pressure at this step. Trilayers were annealed at 760 Torr, 2 Torr, and 0.675 Torr respectively to produce optimally doped, underdoped, and further underdoped YBCO layers.

The lattice structure and orientation of the samples were confirmed using x-ray diffraction measurements. XRR measurements were used to corroborate the thicknesses and roughnesses of the layers and interfaces respectively. XRD and XRR measurements were done on a Rigaku Smartlab using the θ-2θ configuration. XRD scans of the trilayers show peaks associated with the substrate and YBCO, and XRR measurements show intensity oscillations consistent with AFM-established layer thicknesses for all constituent layers. Trilayer T_cs were obtained from their Resistance (R) vs. temperature (T) behaviour, which was measured using a He-4 cryostat and an AC resistance bridge. Electrical contacts for these measurements were placed on the samples in the Kelvin configuration using silver paint. XAS measurements were performed in the UE46-PGM1 beamline of BESSY II at Helmholtz Zentrum Berlin and were acquired in total fluorescence mode with E//ab (LV) polarization.

3. Results and discussion

Fig. 1 plots normalized R vs. T curves of three LCMO trilayers. The T_c, defined as the midpoint of the superconducting transition, is lowered from 73 K to 27 K as the annealing pressure is decreased. The superconducting transition also progressively broadens as the trilayers are underdoped, which indicates increased disorder in the YBCO layer with oxygen underdoping [11,13]. Since all constituent layers are held at 10 nm for all three trilayers, any changes in T_c can reasonably be attributed to differences in p only. Any effect on T_c from the LCMO layers can be assumed to be the same in all three LCMO trilayers. Overall, the attenuation of T_c in these LCMO trilayers is due to a combination of strain mechanisms (strain-induced deoxygenation, intergrowths), which should also appear in the similarly strained LNO trilayers, and magnetic mechanisms from the ferromagnetism of the LCMO layers.

Fig. 2 shows normalized R vs. T curves of three LNO trilayers. Blue, orange, and green curves denote trilayers annealed at 760 Torr, 2 Torr, and 0.675 Torr respectively. The superconducting transitions of the LNO trilayers occur at similar temperatures and with similar transition widths as similarly-annealed LCMO trilayers. Unlike ferromagnetic LCMO, LNO is a paramagnetic metal [19] and is not expected to host a F/S proximity effect, long-range or otherwise. Thus, the similarity in T_c attenuation between the LCMO and LNO trilayers indicates that strain

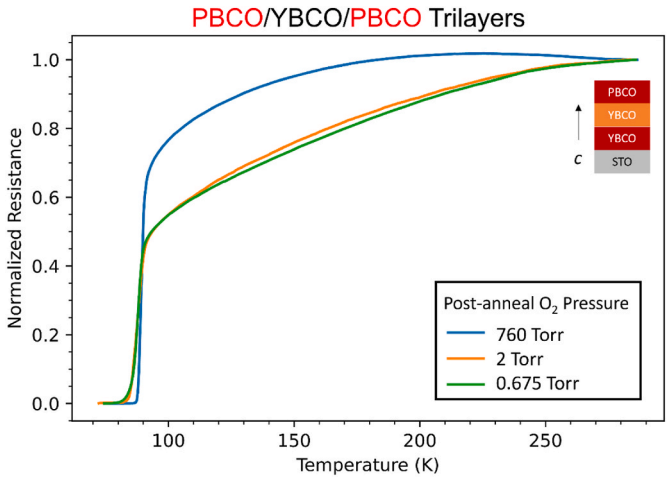

Fig. 3. Normalized R vs. T plots of PBCO trilayers with 10 nm PBCO and YBCO layers. The exact trilayer layout is shown in the inset. The R curves are normalized through division by the room temperature R value of the corresponding trilayer. Unlike the LCMO and LNO trilayers, the superconducting transitions of all three PBCO trilayer samples occur at temperatures close to those seen in single-layer YBCO thin films and only mildly decrease with oxygen underdoping.

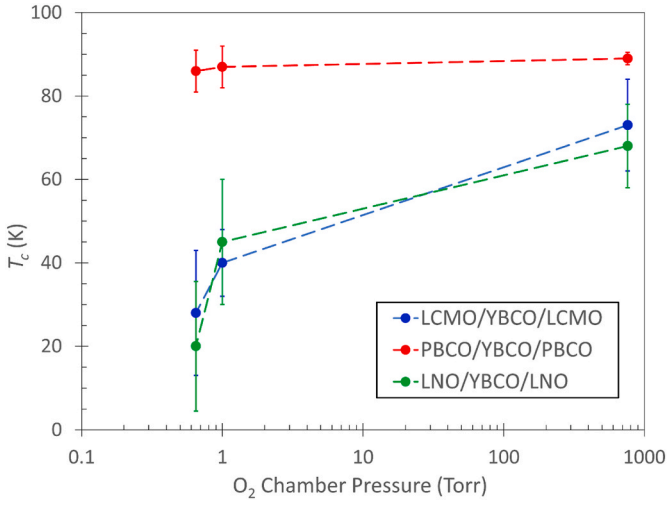

Fig. 4. Plot of T_c vs. O_2 annealing pressure for all three sets of trilayers. Plotted points refer to the midpoint of the superconducting transition, while vertical error bars span the superconducting transition width. The top/bottom of the vertical error bars corresponds to the onset and completion of the superconducting transition respectively. Dashed lines serve as guides to the eye.

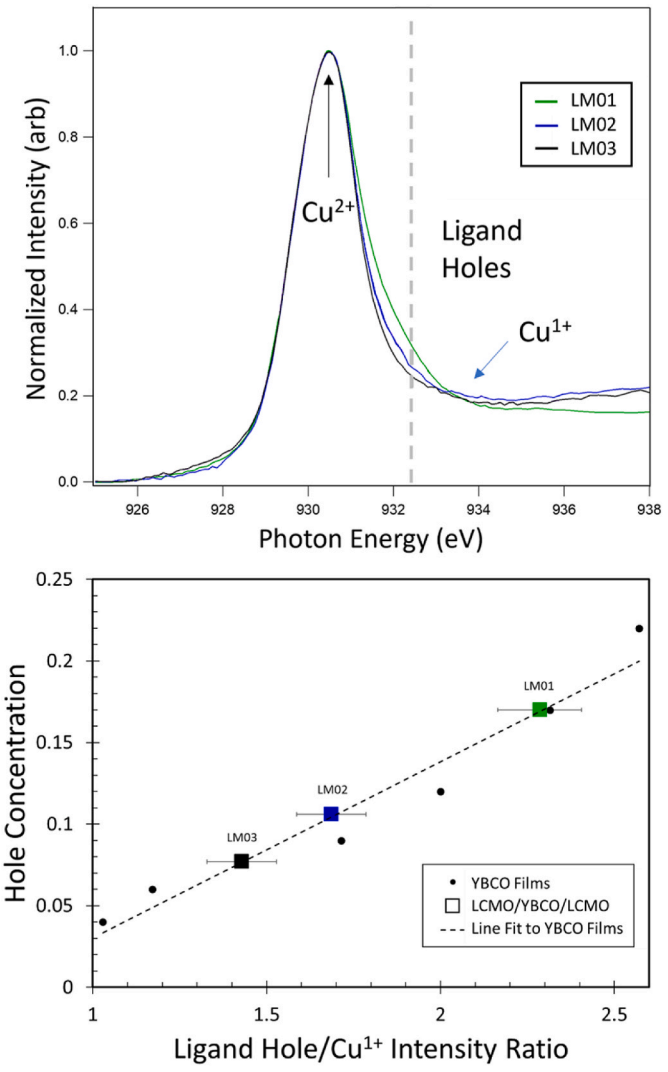

Fig. 5. (top) Normalized XAS measurements at the Cu-L_3 edge of three LCMO trilayers, where the Cu^{2+} (930.6 eV), ligand hole (932.3 eV), and Cu^{1+} features (933.4 eV) are labelled. The intensity ratio of the ligand hole and Cu^{1+} features is used to extract p of the trilayer. (bottom) Plot of p as a function of the ligand hole/Cu^{1+} intensity ratio. Black circles plot the ligand hole/Cu^{1+} ratio and p of YBCO thin films (adapted from Ref. [23]). The linear fit of the YBCO thin film data (dashed black line) allows us to extract p from this ligand hole ratio. Coloured squares plot the ratio and p of the three labelled LCMO trilayers (LM01, LM02, and LM03). Refer to Table 1 for their configurations. Horizontal error bars are propagated from the uncertainties in the intensity and position of the ligand hole and Cu^{1+} features.

mechanisms are primarily responsible for the observed T_c attenuation in both sets of trilayers.

Fig. 3 shows the normalized R vs. T curves of three PBCO trilayers. Similar to Figs. 1 and 2, blue, orange, and green curves denote trilayers annealed at 760 Torr, 2 Torr, and 0.675 Torr respectively. Unlike the previous cases, the T_cs of all PBCO trilayers are close to those of optimally-doped YBCO [20] and only mildly change with decreasing annealing pressure (dropping from 91 K to 82 K as the annealing pressure decreases from 760 Torr to 0.675 Torr). This relatively mild change in T_c indicates that the YBCO layer in the PBCO trilayers is more oxygenated than similarly annealed LCMO and LNO trilayers. This increase in the oxygen uptake rate is physically consistent with the small in-plane lattice mismatch between PBCO and YBCO [13,22].

The T_c vs. annealing pressure behaviour for all three sets of trilayers is plotted in Fig. 4. Vertical error bars represent the superconducting transition widths of the samples. The similarity between the blue and green curves (LCMO and LNO trilayer set respectively) indicates that strain-induced deoxygenation of the YBCO layer is responsible for their T_c attenuation. A comparison with the red curve, representing the more lattice-matched PBCO trilayers, further reinforces this interpretation. The red curve being above and "flatter" than the blue and green curves is consistent with increased oxygen uptake in the YBCO layer of PBCO trilayers. Any magnetic mechanism of T_c suppression should shift the blue curve downwards relative to the green and red curves since only the LCMO layers are ferromagnetic. However, this downshift is not present. The absence of this downshift shows the lack of a significant magnetic mechanism for attenuating superconductivity in LCMO trilayers.

Next, we use XAS to gauge the p values of several LCMO trilayers directly. Fig. 5 shows the extracted p of these trilayers. These values were extracted from XAS measurements using a ratio of their respective

Table 1
List of LCMO trilayers measured by XAS. All LCMO layers are set at 10 nm. The annealing pressure is used to tune the oxygen deficiency of the YBCO layer. The T_c value is the midpoint of the superconducting transition as measured through R vs. T measurements, with the respective error bars denoting the superconducting transition width. The R vs. T behaviour LM02 and LM03 correspond to the blue and orange curves of Fig. 1 respectively.

Sample	YBCO Layer (nm)	Anneal Pressure (Torr)	T_c (K)
LM01	50	760	88 ± 2
LM02	10	760	73 ± 8
LM03	10	2	40 ± 9

ligand hole/Cu^{1+} intensities. Here, we use the linear relationship between the intensity of the ligand hole feature and p [23] to obtain p values for the samples. Normalizing the intensity of the ligand hole feature by the intensity of the Cu^{1+} feature is necessary to allow for comparisons between different sets of XAS data. Three LCMO trilayers were measured using XAS. Their YBCO thicknesses and anneal pressures are tabulated in Table 1 and span both the YBCO thickness and doping parameter spaces. LM01 is a trilayer with a relatively thicker YBCO layer that shows a T_c close to that of optimally doped single-layer YBCO thin films. In comparison, LM02 and LM03 are trilayers with much thinner YBCO layers that are oxygen underdoped to different degrees.

We find a significantly lower p value in LM01 compared to LM02, which indicates that p decreases with thinner YBCO in LCMO trilayers even when both trilayers are nominally optimally doped. This significant decrease in p occurs with YBCO and LCMO layer thicknesses within the length scale of the proposed long-range F/S proximity effect. Combined with the similarity in T_c attenuation between the LCMO and LNO trilayers, our results indicate that strain-induced deoxygenation of the YBCO layer is primarily responsible for the observed T_c reduction in LCMO trilayers at the length scales governed by the proposed long-range F/S proximity effect.

4. Conclusion

We compared changes in T_c as a function of annealing pressure in c-axis LCMO, LNO, and PBCO trilayers. This comparison was made to distinguish between the effects of strain-induced deoxygenation and any magnetic mechanisms on the attenuation of superconductivity in LCMO trilayers. We found similar T_c attenuation in similarly-treated LCMO and LNO trilayers, which indicated that strain-induced deoxygenation is primarily responsible for the observed T_c attenuation in both LCMO and LNO trilayers. The milder attenuation of T_c in similarly-treated PBCO trilayers reinforces this interpretation. We also directly gauged the p of several LCMO trilayers using XAS, which showed lower p values in LCMO trilayers with thinner YBCO layers. Our results indicate that any magnetic mechanisms on the superconductivity, including the proposed long-range F/S proximity effect, are superfluous in LCMO/YBCO multilayers.

Declaration of competing interest

The authors declare that they have no known competing financial interests or personal relationships that could have appeared to influence the work reported in this paper.

Acknowledgements

This work is supported by the Natural Sciences and Engineering Research Council of Canada, the Canada Foundation for Innovation, and the United States Air Force Office of Scientific Research Young Investigator Program under grant FA9550-19-1-0063.

References

[1] A.M. Goldman, V. Vas'ko, P. Kraus, K. Nikolaev, V.A. Larkin, Cuprate/manganite heterostructures, J. Magn. Magn Mater. 200 (1999) 69–82.
[2] Z. Sefrioui, D. Arias, V. Peña, J.E. Villegas, M. Varela, P. Prieto, C. León, J. L. Martinez, J. Santamaria, Ferromagnetic/superconducting proximity effect in $La_{0.7}Ca_{0.3}MnO_3/YBa_2Cu_3O_{7-\delta}$ superlattices, Phys. Rev. B 67 (21) (2003), 214511.
[3] V. Pena, Z. Sefrioui, D. Arias, C. Leon, J. Santamaria, M. Varela, S.J. Pennycook, J. L. Martinez, Coupling of superconductors through a half-metallic ferromagnet: evidence for a long-range proximity effect, Phys. Rev. B 69 (2004), 224502.
[4] J. Chakhalian, J.W. Freeland, H.-U. Habermeier, G. Cristiani, G. Khaliullin, M. Van Veenendaal, B. Keimer, Orbital reconstruction and covalent bonding at an oxide interface, Science 318 (2007) 1114–1117.
[5] A. Frano, S. Blanco-Canosa, E. Schierle, Y. Lu, M. Wu, M. Bluschke, M. Minola, G. Christiani, H.U. Habermeier, G. Logvenov, others, Long-range charge-density-wave proximity effect at cuprate/manganate interfaces, Nat. Mater. 15 (2016) 831–834.
[6] A.I. Buzdin, Proximity effects in superconductor-ferromagnet heterostructures, Rev. Mod. Phys. 77 (3) (2005) 935–976.
[7] Y. Tanaka, Y. Tanuma, A.A. Golubov, Odd-frequency pairing in normal-metal/superconductor junctions, Phys. Rev. B 76 (2007), 054522.
[8] S. Kawabata, Y. Asano, Y. Tanaka, A.A. Golubov, Robustness of spin-triplet pairing and singlet–triplet pairing crossover in superconductor/ferromagnet hybrids, J. Phys. Soc. Jpn. 82 (2013), 124702.
[9] P. Högl, A. Matos-Abiague, I. Žutić, J. Fabian, Magnetoanisotropic andreev reflection in ferromagnet-superconductor junctions, Phys. Rev. Lett. 115 (11) (2015), 116601.
[10] I. Fridman, L. Gunawan, G.A. Botton, J.Y.T. Wei, Scanning tunneling spectroscopy study of c-axis proximity effect in epitaxial bilayer manganite/cuprate thin films, Phys. Rev. B 84 (10) (2011), 104522.
[11] H. Zhang, N. Gauquelin, G.A. Botton, J.Y.T. Wei, Attenuation of superconductivity in manganite/cuprate heterostructures by epitaxially-induced CuO intergrowths, Appl. Phys. Lett. 103 (2013), 052606.
[12] H. Zhang, A. Nguyen, T. Gredig, J.Y.T. Wei, Strain-driven attenuation of superconductivity in heteroepitaxial perovskite/YBCO/perovskite thin films, arXiv 1710 (2017), 10668.
[13] I. Bozovic, G. Logvenov, I. Belca, B. Narimbetov, I. Sveklo, Epitaxial strain and superconductivity in $La_{2-x}Sr_xCuO_4$ thin films, Phys. Rev. Lett. 89 (10) (2002), 107001.
[14] H.B. Peng, B.R. Zhao, Z. Xie, Y. Lin, B.Y. Zhu, Z. Hao, H.J. Tao, B. Xu, C.Y. Wang, H. Chen, F. Wu, Ordered surface structure in $La_{1-x}Ca_xMnO_3$ films, Phys. Rev. Lett. 82 (2) (1999) 362–365.
[15] L.S.-J. Peng, X.X. Xi, B.H. Moeckly, S.P. Alpay, Strain relaxation during in situ growth of $SrTiO_3$ thin films, Appl. Phys. Lett. 83 (2003) 4592–4594.
[16] T. Wang, K. Ganguly, P. Marshall, P. Xu, B. Jalan, Critical thickness and strain relaxation in molecular beam epitaxy-grown $SrTiO_3$ films, Appl. Phys. Lett. 103 (2013), 212904.
[17] T.L. Meyer, L. Jiang, S. Park, T. Egami, H.N. Lee, Strain-relaxation and critical thickness of epitaxial $La_{1.85}Sr_{0.15}CuO_4$ films, Apl. Mater. 3 (2015), 126102.
[18] M.J. Sayagués, M. Vallet-Regı, A. Caneiro, J.M. González-Calbet, Microstructural characterization of the $LaNiO_{3-y}$ system, J. Solid State Chem. 110 (1994) 295–304.
[19] R.D. Sánchez, M.T. Causa, J. Sereni, M. Vallet-Regí, M.J. Sayagués, J.M. González-Calbet, Specific heat, magnetic susceptibility and electrical resistivity measurements on $LaNiO_3$, J. Alloys Compd. 191 (1993) 287–289.
[20] R. Liang, D.A. Bonn, W.N. Hardy, Evaluation of CuO_2 plane hole doping in $YBa_2Cu_3O_{6+x}$ single crystals, Phys. Rev. B 73 (18) (2006), 180505.
[21] J.L. Tallon, C. Bernhard, H. Shaked, R.L. Hitterman, J.D. Jorgensen, Generic superconducting phase behavior in high-T_c cuprates: T_c variation with hole concentration in $YBa_2Cu_3O_{7-\delta}$, Phys. Rev. B 51 (18) (1995) 12911–12914.
[22] H.B. Radousky, A review of the superconducting and normal state properties of $Y_{1-x}Pr_xBa_2Cu_3O_7$, J. Mater. Res. 7 (1992) 1917–1955.
[23] Y.-J. Chen, M.G. Jiang, C.W. Luo, J.-Y. Lin, K.H. Wu, J.M. Lee, J.M. Chen, Y.K. Kuo, J.Y. Juang, C.-Y. Mou, Doping evolution of Zhang-Rice singlet spectral weight: a comprehensive examination by x-ray absorption spectroscopy, Phys. Rev. B 88 (13) (2013), 134525.